Comparative Analysis of the NACA 4412 Airfoil for Subsonic and Transonic Flow Using Artificial Neural Networks Based on Bayesian Regularization Method

Mamoon Aamir[1], Aqsa Zafar Abbasi[2, *]

[1]Department of Aeronautics and Astronautics, Institute of Space Technology, Islamabad, Pakistan, mamoonaamir08@gmail.com

[2]Department of Applied Mathematics and Statistics, Institute of Space Technology, Islamabad, Pakistan, zafariqbalabbasi67@gmail.com

** Corresponding author; E-mail: zafariqbalabbasi67@gmail.com*

Submitted 25/01/2026, Accepted 03/06/2026, Available online 29/11/2026, Published 30/06/2027
DOI: 10.64518/uohjs.2027.01

Abstract:
This paper offers a scientifically informed surrogate model to make predictions about the aerodynamic response of NACA 4412 airfoil via an Artificial Neural Network (ANN) that has been trained with Bayesian Regularization. XFLR5 was used to in compressible and high Mach conditions to create aerodynamic datasets at Reynolds number of $1 * 10^5$. *Angle of attack and Mach number are the input parameters, whereas the lift, drag and pitching moment coefficients are the outputs. It has a single- hidden-layer feed-forward neural network that has 20 neurons as its hidden layer. The detailed sensitivity analysis was performed to assess the overall influence of the hidden neurons, the functions of activation and data partitioning on the model performance. The ANN surrogate model was of high predictive capability with the coefficients of determination* $R^2 > 0.99$ *when predicting the lift coefficient and low error values of all aerodynamic outputs. The predicted aerodynamic trends namely the linearity of lift curve, the stall characteristics and the increase in drag were observed to be in agreement with the known literature. The findings demonstrate that ANN-based surrogate models are effective as computationally efficient in estimating aerodynamic behavior. The study also discusses the limitations associated with the use of panel-method-based datasets and outlines directions for future work involving high-fidelity CFD and experimental validation.*

Keywords: NACA 4412; aerodynamic surrogate model; XFLR5; artificial neural network; Bayesian regularization.

1. Introduction

The NACA 4412 airfoil, a cambered member of the NACA four-digit series, was selected for this study;

1.1. NACA Four-Digit Series

Engineers and designers may more easily generate and analyze airfoil profiles due to a technique used to determine the geometric characteristics of airfoil forms called the NACA (National Advisory Committee for Aeronautics) four-digit airfoil series. The NACA designation's four numbers stand for many things:

First Digit (Maximum Camber): The upper surface of the airfoil is curved, and the first digit denotes its maximum camber. This number denotes the region of the chord length where the greatest camber is observed. The maximum camber, for example, in NACA 4412 is 4% of the chord length.

Second Digit (Position of Maximum Camber): The greatest camber along the chord is denoted by the second digit, which is given as a percentage of the chord length. The maximum camber of the identical NACA 4412 sample is located at 40% of the chord.

Last Two Digits (Maximum Thickness): The airfoil's maximum thickness is represented by the final two figures as a percentage of chord length. The maximum thickness of the NACA 4412 airfoil is 12% of the chord length.

In short The first digit gives maximum camber as a percentage of chord; the second gives its position in tenths of chord; the last two give maximum thickness as a percentage of chord. Wind energy continues to progress as an indigenous and efficient energy source, despite numerous concerns about wind turbine noise (Kaldellis and Kapsali, 2013; Ledo et al., 2011). As a result, aerodynamic studies frequently look at ways to improve the efficiency of wind turbine airfoils. Low Reynolds number airfoils are those used in wind turbines that operate at Reynolds numbers less than 5x 10^5 (Carmichael, 1981). Low Reynolds numbers are often when harmful airfoil performance events like leading-edge separation developing or laminar separation bubble (LSB) take place. Due to low pressure gradients, the laminar flow may split from the airfoil's surface. When the flow changed from laminar to turbulent, the separated laminar flow rejoined at the trailing edge of the airfoil. The region between the sites of detachment and reattachment was referred to as LSB (Genç, 2012). A loss of aerodynamic performance, a disproportionate rise in drag coefficient, vibration, and noise are all effects of LSB (Genç et al., 2012; Sahin et al., 2008; Clausen and Wood, 1999; Miley, 1982). Based on an experimental research, Wahidi et al. (2012) examined the impact of flow phenomena over a NACA 4412 airfoil at a Reynolds number of 5x104 and different angles of attack (α). According to their findings, V3V and PIV, roll-up vortices along the spanwise formed pairs of both negative and positive wall-normal velocity, that are crucial in terms of reconnecting zone destabilization. Wahidi and Bridges' (2009) investigation involved measurements of the surface pressure as well as boundary layer at Reynolds numbers of 15×10^4 and 25×10^4 for NACA 0012 and LA2573a airfoils. According to their results, the length of the LSB decreased as the Reynolds number rose. Although changing the angle of attack reduced the length of the bubble on LA2573a between α =0 ° and α =2 °, it did not considerably reduce the length of the bubble on the NACA 0012 airfoil. On a NACA 663-018 airfoil with chord Reynolds numbers varying from 5×10^4 to 2×10^5 and angles of attack between 8° and 12°, O'Meara and Mueller (1987) demonstrated LSB. According to the study, LSB's length and thickness decreased as Reynolds number increased. However, when the angle of attack was raised from 10° to 12°, the LSB's thickness and length grew. In addition to formation LSB, the chord Reynolds number as well as disturbance environment had an impact on the experimental pressure distribution. Based on numerical modeling, Alam and Sandham (2000) treated short LSB in two and three dimensions. Three-dimensional simulation was used to explore the transition to a turbulent process. Calculated results showed that the laminar boundary layer was forced to separate. By passing through the divided pressure layer, the transition start was observed. Additionally, turbulence instances dominated the turbulent kinetic energy budget in the reattachment zone. However, a two-dimensional simulation could not have properly depicted the creation of a brief bubble. Yarusevych et al. (2004) experimentally investigated the boundary layer growth on the NACA 0025 airfoil at Reynolds numbers of 1 $\times 10^5$ and 1.5 $\times 10^5$. Results showed that at a Reynolds number of 1.5 $\times 10^5$, a brief LSB took place in the boundary layer. However, the NACA 0025 airfoil's split shear layer failed to surface at Reynolds numbers of 1×10^5, and a broader wake that significantly reduced the performance of the airfoil was created. Based on the experimental work, Hu and Yang (2008) examined into the transient behavior of laminar flow separation over a NASA low-speed GA (W)-1 airfoil. According to the results of experiments, boundary layer separation took place at an angle of $\alpha \geq 8°$. When the unfavorable pressure gradient was great enough at $\alpha < 12°$, the separated boundary layer reattached to the surface of the airfoil, resulting in the creation of LSB. Additionally, it was determined that raising the LSB had an adverse effect on the aerodynamic performance of the airfoil since the lift coefficient was found to be drastically reduced and the drag coefficient to increase.

1.2. Artificial Neural Networks

The human brain contains massive neural networks which are capable of executing intellectual, perception, and behavioral tasks at which humans excel. The brain is capable of conducting computationally complicated perceptual operations (such as face recognition and speech recognition) as well as controlling activities (such as movement of the body and operations). The brain's strength comes from its effective use of massive parallelism, a highly efficient processing structure. as well as the limited information-processing skills. The brain of an individual is a structure made up of approximately 10 billion interconnected neurons. Each neuron is a cell that receives, analyses, and releases data through biological responses. Dendrites are nerve fiber networks that look like trees. The cell nucleus is connected to the cell's body or soma. The axon is an individual long fiber that stretches from the cell body and eventually forks into threads and sub-strands that connect to neighboring neurons. Message transmission across synapses is a complex chemical process in which specific transmitter molecules are created on the receiving side of the synapse. As a result, the potential for electricity within the cell that receives it cell's body increases or decreases. When the voltage hits a particular threshold, a pulse is conveyed down the axon and the cell "fires". As generalizations of mathematical representations of organic nerve systems, artificial neural networks (ANN) were developed. Many ANNs are used in engineering tasks such as recognizing patterns, projections, and data diminution, as well as simulating real neural networks for investigating animal and machine behavior and control. AI-based computing stochastic numerical algorithms have been used in published research in a variety of fields (Abbasi et al., 2025a; Raja et al., 2025; Abbasi et al., 2025b; Aamir et al., 2025; Abbasi et al., 2026; Aamir et al., 2026; Shoaib et al., 2022).

The aerodynamic behavior of the NACA 4412 airfoil has been extensively studied using CFD and experimental methods in the literature; therefore, the present work focuses on evaluating the capability of ANN-based surrogate models to learn and reproduce these aerodynamic relationships. The goal of this study is to give an examination of the NACA 4412 airfoil utilizing artificial neural networks (ANNs) and the Bayesian Regularization approach (BRA). The following are the contributions and novel insights of the computing stochastic numerical procedures:

- An innovative computational stochastic numerical approach Bayesian Regularization based on neural networks (BRNNAI) is presented viably for the study of NACA 4412 airfoil.
- The ability of XFLR5 is utilized to generate data samples for testing, validating, and training BRNNAI to build networks for the NACA 4412 airfoil.
- The exact and constant overlapping of the computational findings in excellent agreement with conventional solutions with small absolute error (AE) validates the utility of the airfoil by BRNNAI.
- The computational stochastic technique is supported by analysis using error histograms (EH), MSE-based convergence curves, correlation, and regression.
- The comparison of NACA 4412 for subsonic and transonic on the basis of angle of attack and coefficient of moment have done.
- Comprehensive sensitivity analysis of ANN hyperparameters.

The remaining part of the article is structured as follows: Section 2 labels the essential parameters for airfoil analysis. Section 3 describes the numerical performances of BRNNAI. Section 4 contains the results as well as future recommendations.

2. Aerodynamic Parameters

2.1. Reynolds Number

The Reynolds number is a dimensionless parameter that is used in many fluid dynamics situations to determine the density, viscosity, speed, and size of typical flows. This dimensionally neutral number or combination commonly develops in connection with the observation of turbulent or laminar flow.

2.1.1. Laminar Flow (Low Reynolds Number)

The flow shows an ability to be regular and smooth when the Reynolds number is low, usually under 2,000, with the fluid particles flowing in parallel layers. This regime is dominated by viscous forces.

2.1.2. Turbulent Flow (High Reynolds Number)

Reynolds numbers frequently exceed a critical point between 4,000 and 6,000, after which the flow becomes chaotic and disordered with vortices, eddies, and mixing as a result. Viscous forces are subordinate to inertial forces in this regime.

2.2. Lift Coefficient

The lift generated by an airfoil or aircraft as it travels through a fluid, usually air, is measured by the dimensionless coefficient known as C_L. It is defined as the lift force, which is the force perpendicular to the relative airflow, to the product of the reference area of the airfoil or aircraft, the fluid's dynamic pressure, and a coefficient (usually 0.5 for incompressible flow). In mathematics, it is written as:

$$C_L = \frac{L}{0.5\rho V^2 A} \tag{1}$$

2.3. Drag Coefficient

In cases where an object is moving in a fluid medium, the resistance capacity of the fluid is measured by the Drag Coefficient C_D which is divided by the frontal cross-section of the object. This parameter is used by aerodynamicists to model the effect of geometric configuration, angular orientation and fluid flow properties on the aerodynamic resistance forces. Mathematically C_D defined as:

$$C_D = \frac{D}{0.5\rho V^2 A} \tag{2}$$

2.4. Angle of Attack (α)

The angle of attack (AOA), defined as the angle produced by the line of the chord of the airfoil and the entering airflow, is directly related to the coefficient of lift (C_L). The C_L fluctuates as the angle of attack varies.

3. Methodology and Results

For the NACA 4412 airfoil, the suggested computing stochastic numerical approach is supplied in two parts.

- For the computing stochastic numerical process based BRNNAI, critical and extensive explanations are presented.
- The implementation techniques aid in the computation of the stochastic numerical procedure for the NACA 4412 airfoil.

3.1. Data Generation and Aerodynamic Parameters

The aerodynamic dataset used in this study was generated using the XFLR5 aerodynamic analysis tool. The NACA 4412 airfoil was analyzed at a Reynolds number of Re=1×10^5 with a critical amplification factor of Ncrit=9.

The angle of attack was varied from −10° to 15° with a step size of 0.5°, resulting in a dataset that captures both pre-stall and post-stall aerodynamic behavior.

The following aerodynamic coefficients were obtained:

- Lift coefficient C_L
- Drag coefficient C_D

- Pitching moment coefficient C_m

All these aerodynamic quantities are the neural network model output targets.

The data were divided into training, testing, and validation subsets in a 70:25:5 ratio.

3.2. Artificial Neural Network Model

To model this nonlinear relationship between the aerodynamic parameters and the performance of airfoils, a feed-forward artificial neural network with Bayesian Regularization was employed as a surrogate regression model.

The ANN architecture consists of:

- Input layer
- Hidden layer with **20 neurons**
- Output layer

The **log-sigmoid activation function** was used in the hidden layer, while a linear activation function was used in the output layer.

Bayesian Regularization backpropagation algorithm was used to complete network training with an objective function that is modified with a regularization term to enhance the ability to generalize.

The cost functional of training is given as:

$$F = \alpha E_d + \beta E_w \tag{3}$$

where

E_d denotes the squared error between target and predicted value and

E_w is the addition of squared network weights.

Automated adjustment of the parameters of α and β during training works to balance the data fitting and model complexity.

3.3. Sensitivity Analysis of ANN Hyperparameters

To test the strength of the suggested artificial neural network model, a sensitivity analysis was carried out to change several principal hyperparameters such as the size of hidden neurons, source functions, and divide techniques.

3.3.1. Effect of Hidden Neurons

The hidden layer has greatly an influence in the number of neurons, which influences the predictive ability of the neural network. Few neurons can result in underfitting, and many neurons can result in overfitting and more computation. To examine this effect, 5, 10, 15, 20, 25, and 30 hidden neurons networks were tried. Based on the mean square error (MSE) metric, the performance of every configuration was compared. The findings show that networks that have less than 10 neurons have comparatively bigger prediction errors since such models have inadequate capacity. The more neurons, the higher is prediction accuracy to a level of about 20 neurons, and further addition of neurons only provides a small boost to prediction at a higher computational cost. Thus, the number of selected hidden neurons was 20, the most appropriate one in the current research.

3.3.2. Effect of Activation Functions

The activation functions are important in capturing nonlinearities of variation between input and output variables. Three of the most frequently utilized activation functions were tested:

- Log-sigmoid function
- Hyperbolic tangent sigmoid (tanh)
- Rectified Linear Unit (ReLU)

The results demonstrate that the log-sigmoid activation function provided the lowest prediction error and the most stable convergence behavior during training using Bayesian Regularization. Tanh function showed similar results but needed a few more training iterations, whereas ReLU function did not show as stable convergence on the data in question.

As a result, the final ANN architecture is the choice of the log-sigmoid activation function in the log- sigmoid hidden layer.

3.3.3. Effect of Dataset Partition

The effect of dataset partition on the model performance was also examined. Three data split strategies were taken into account:

- 70% training – 25% testing – 5% validation
- 80% training – 10% testing – 10% validation
- 60% training – 20% testing – 20% validation

The results show that increasing the training data generally improves model learning capability, while maintaining sufficient testing data is necessary for unbiased performance evaluation.

Out of the best configurations which were evaluated, the 70-25-5 split offered the most balanced performance that guaranteed a sufficient amount of training data without compromising on the independent testing samples.

Overall, the sensitivity analysis demonstrates that the ANN model performance is influenced by the choice of architecture and dataset partition. The configuration consisting of:

- 20 hidden neurons
- Log-sigmoid activation function
- 70–25–5 dataset split

provided the best trade-off between prediction accuracy, convergence stability, and computational efficiency. Tables 1–3 present the sensitivity analysis of ANN architecture based on Neurons, data split and activation functions.

Table 1. Sensitivity Analysis of ANN Architecture

Hidden Neurons	Activation Function	Data Split	MSE
5	Logsig	70-25-5	1.8E-3
10	Logsig	70-25-5	6.4E-4
15	Logsig	70-25-5	1.2E-4
20	Logsig	70-25-5	8.4E-6
25	Logsig	70-25-5	8.2E-6
30	Logsig	70-25-5	8.1E-6

Table 2. Activation Function Comparison

Activation Function	MSE	Convergence Stability
Logsig	8.4E-6	High
Tanh	1.2E-5	Moderate
ReLU	3.5E-5	Low

Table 3. Data Split Sensitivity

Training	Testing	Validation	MSE
60%	20%	20%	1.5E-5
70%	25%	5%	8.4E-6
80%	10%	10%	9.1E-6

3.4. BRNNAI Implementation and Aerodynamic Results

Figure 1 presents an appropriate design process flow framework for the NACA 4412 airfoil employing the computational stochastic numerical methodology. BRNNAI functions through the multi-layers demonstrated in Figure 2. Meanwhile, Figure 3 demonstrates the BRNNAI architecture. The methodology is executed in "MATLAB" with a layer configuration that comprises single input, output, and hidden layers, 20 hidden neurons, n-fold cross validation, 1000 epochs, log-sigmoid activation function, and the Bayesian Regularization optimization algorithm with standard parameters for iteration,

termination criteria, tolerances, and step size. Additionally, reference data for input and objectives are generated through a traditional numerical solution, with 70% of arbitrary data selected for training, 25% for testing, and 5% for validation.

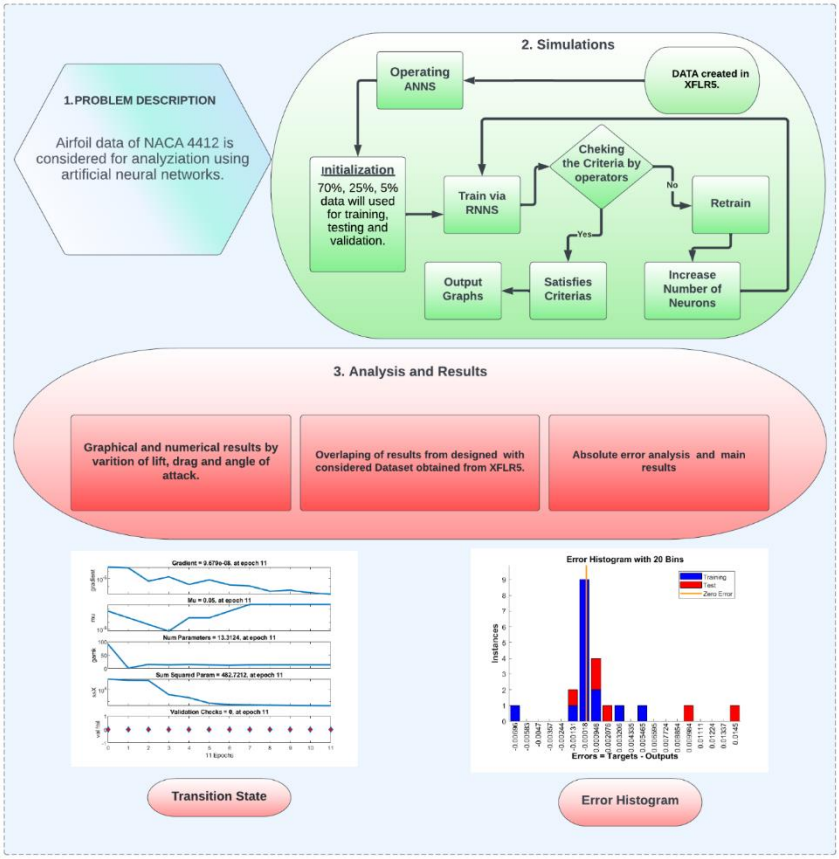

Figure 1. Workflow

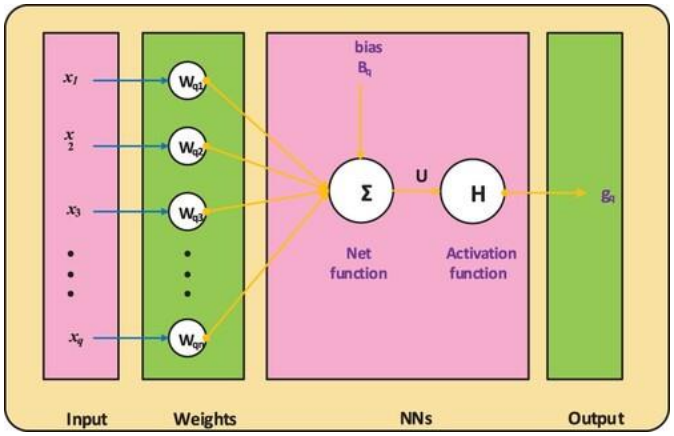

Figure 2. Single neuron framework

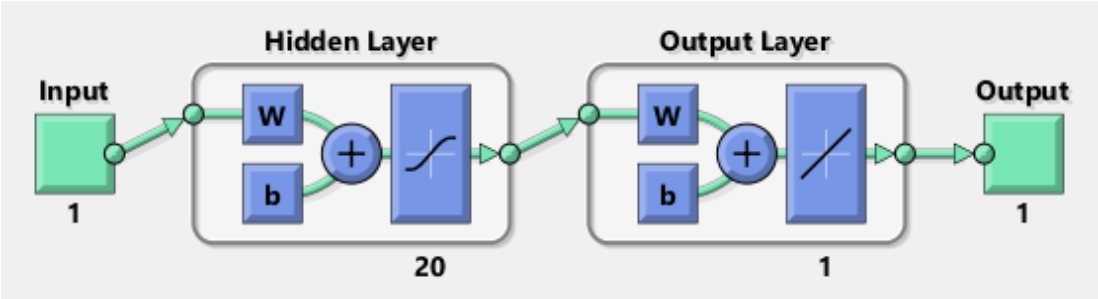

Figure 3. BRNNAI topology

Inspired by relevant recent studies, the suggested Models of neural networks with ten neurons are based on the best possible tradeoff between underfitting and overfitting of neural networks throughout the training and validation process with 1000 epochs. However, in this situation, we use 20 neurons as the starting point to improve accuracy. The BRNNAI procedure's training, testing, and validation samples are picked at random, with 70%, 25%, and 5%, respectively. If we have less training sample, say 40%-60%, the MSE for testing rises from 30% to 40%, resulting in overall bad algorithm performance. On the flip side, if we utilize additional samples for training, such as 90%, 5% for testing and 5% validation, the precision of the procedure small increase for labelled data, i.e. partiality input as well as targets, but the durability of the framework is not thoroughly demonstrated for data that is objective without previous understanding of the targets.

Tables 4–7 represent the simulations of airfoil analysis of NACA4412 under BRNNAI for different scenarios. Table 4 is for C_D vs C_L, Table 5 is for α vs C_L and Table 6 is for α vs C_D. Figures 4–7 shows the graphical illustration of BRNNAI for airfoil analysis of NACA4412 for the scenarios of Tables 4–7 respectively. Figure 4(a)'s performance curve shows that the MSE was 0.349 after 26 epochs. The estimates for gradient and mu are 0.184 and 1.00E+10, respectively, according to training state Figure 4(b). In 4(c-e), the EH, FC, and RA are shown. A performance plot in 5(a) shows that the MSE after 231 epochs is 8.46E-06. According to training state Figure 5(b), the evaluations of gradient and mu are 5.27E-06 and 1.00E+10, respectively. In Figure 5(c-e), the EH, FC, and RA are shown. The performance curve in Figure 6(a) shows that the MSE after 11 epochs was 4.40E-09. The estimates for gradient and mu are 9.68E-08 and 0.05, respectively, according to training state Figure 6(b). In 6(c-e), the EH, FC, and RA are shown. Figure 7(a)'s performance curve shows that the MSE was 8.14 after 100 epochs. The estimates for gradient and mu are 2.98 and 0.0500, respectively, according to training state Figure 7(b). In 7(c-e), the EH, FC, and RA are shown.

Table 4. Simulations of BRNNAI for Airfoil NACA4412 on the basis of C_L vs C_D

Mean Square Error			Performance	Mu Parameter	Gradient	Epochs	Time
Training	Validation	Testing					
4.20666E-2	0.00000E-0	5.09043E-0	0.349	1.00E+10	0.184	26	0s

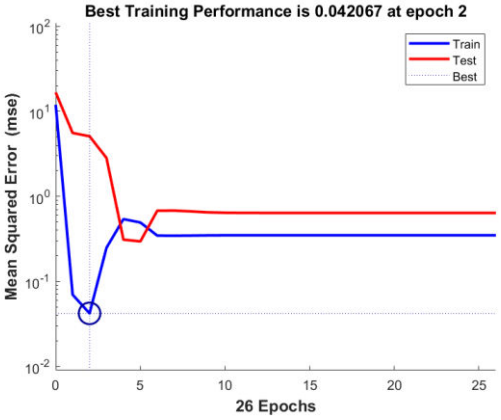

(a) MSE

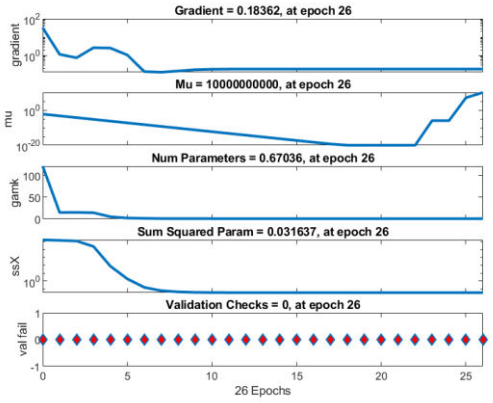

(b) TA

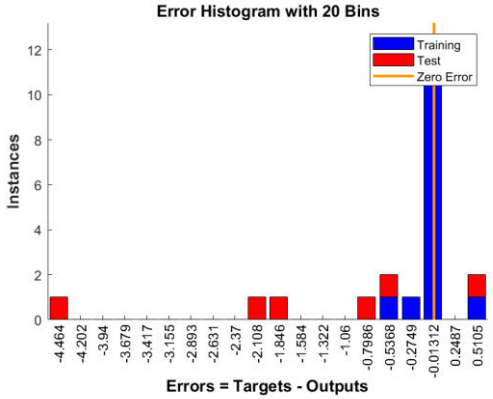

(c) EH

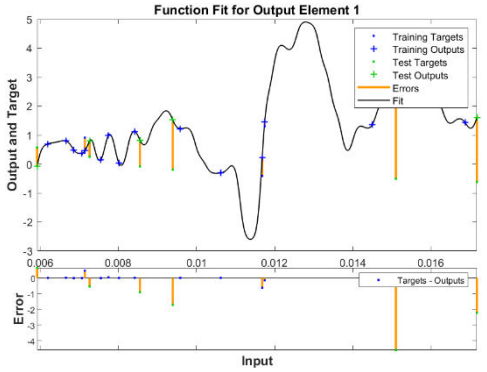

(d) FC

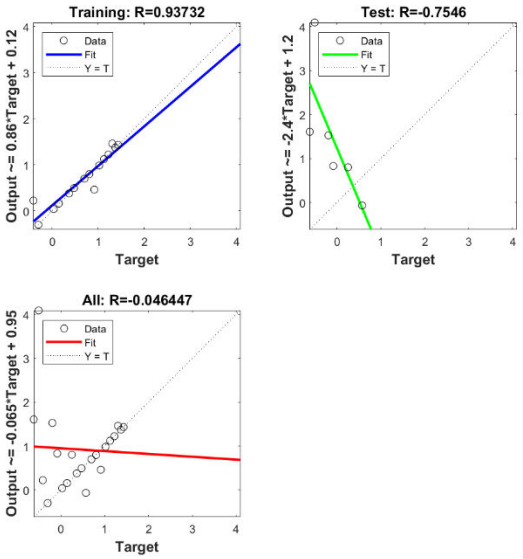

(e) RA

Figure 4. BRNNAI simulations for Airfoil NACA4412 on the basis of C_L vs C_D

Table 5. Simulations of BRNNAI for Airfoil NACA4412 on the basis of C_L vs α

Mean Square Error			Performance	Mu Parameter	Gradient	Epochs	Time
Training	Validation	Testing					
6.47635E-6	0.00000E-0	5.51285E-5	8.46E-06	1.00E+10	5.27E-06	231	0s

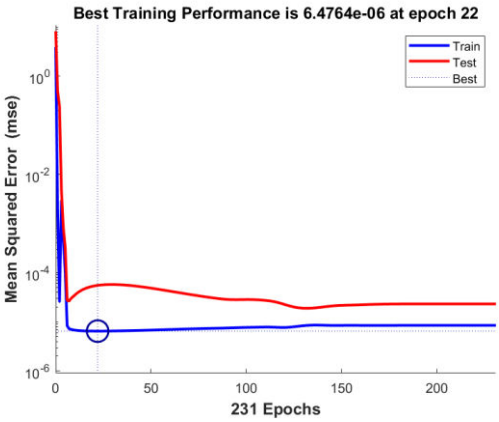

(a) MSE

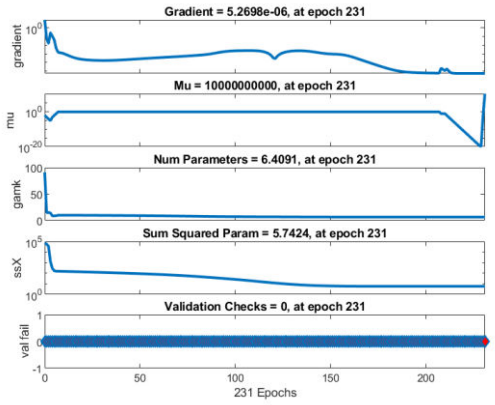

(b) TA

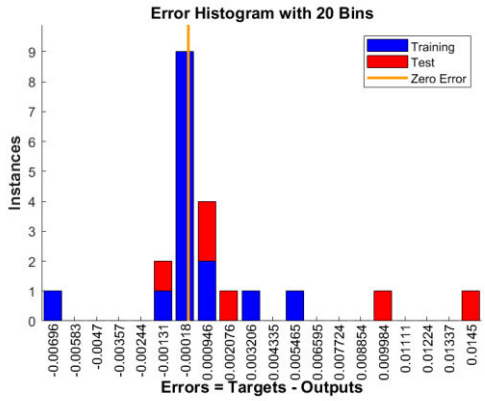

(c) EH

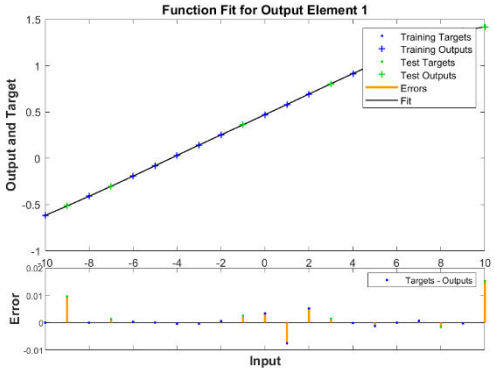

(d) FC

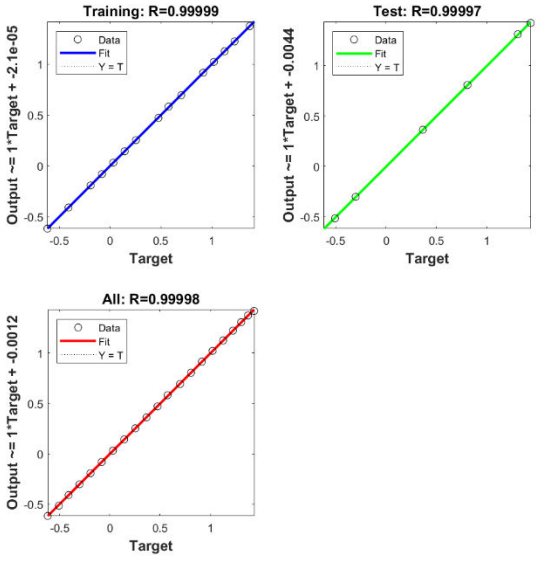

(e) RA

Figure 5. BRNNAI simulations for Airfoil NACA4412 on the basis of C_L vs α

Table 6. Simulations of BRNNAI for Airfoil NACA4412 on the basis of C_D vs α

Mean Square Error			Performance	Mu Parameter	Gradient	Epochs	Time
Training	Validation	Testing					
4.39509E-9	0.00000E-0	1.48029E-7	4.40E-09	0.0500	9.68E-08	11	0s

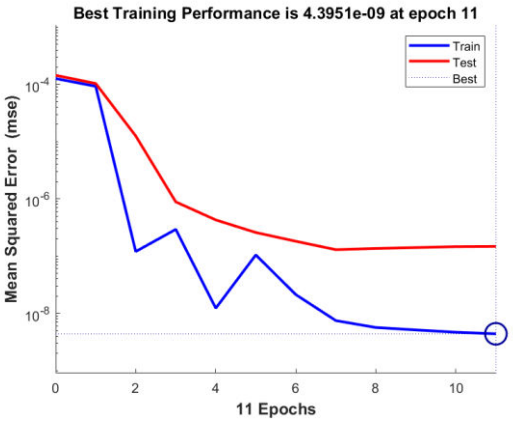

(a) MSE

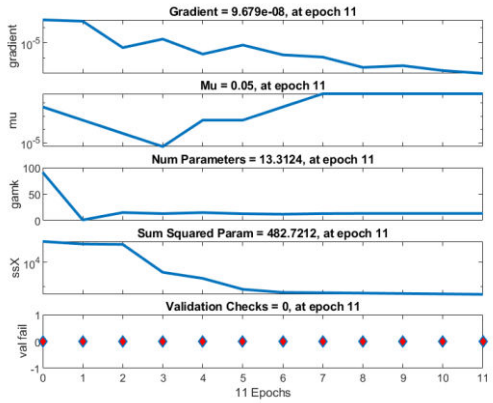

(b) TA

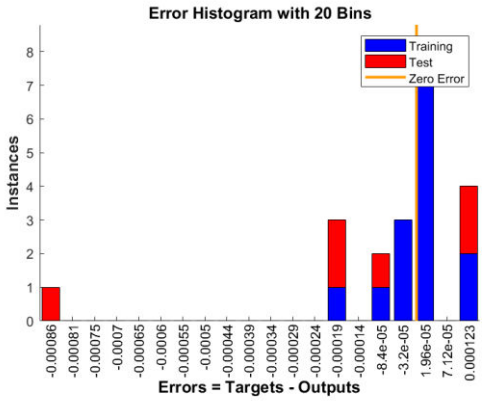

(c) EH

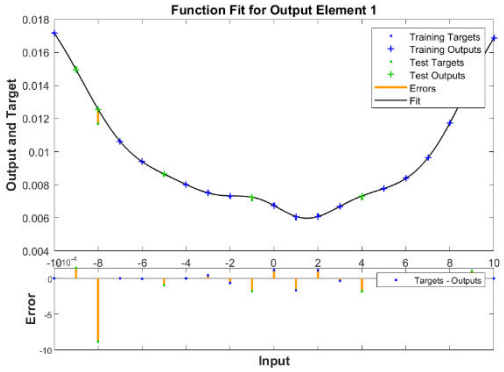

(d) FC

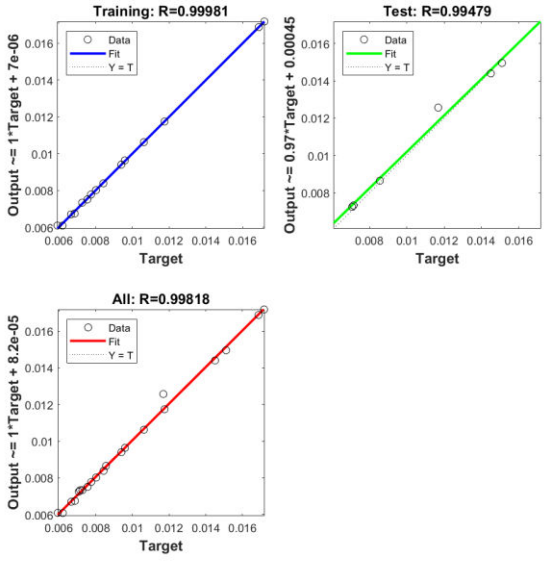

(e) RA

Figure 6. BRNNAI simulations for Airfoil NACA4412 on the basis of C_D vs Alpha(α)

Table 7. Simulations of BRNNAI for Airfoil NACA4412 on the basis of C_L/C_D vs α

Mean Square Error			Performance	Mu Parameter	Gradient	Epochs	Time
Training	Validation	Testing					
8.13471E-0	0.00000E-0	3.42407E-0	8.14	0.0500	2.98	100	3s

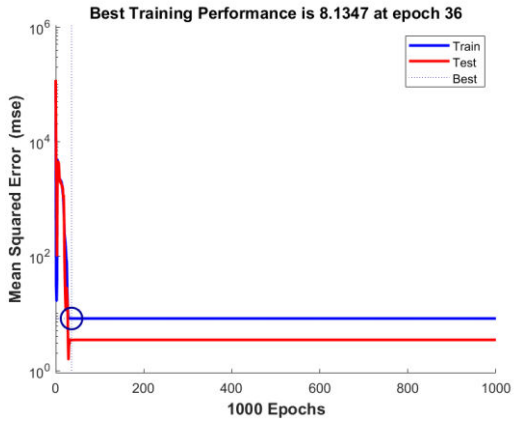

(a) MSE

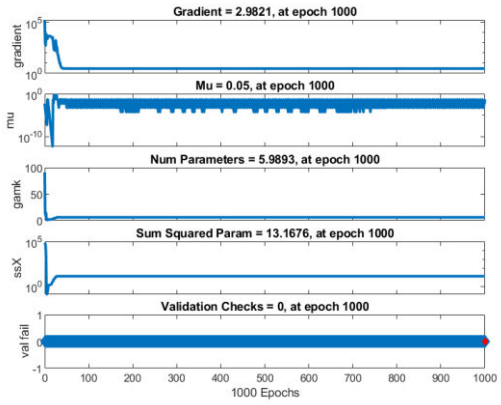

(b) TA



(c) EH

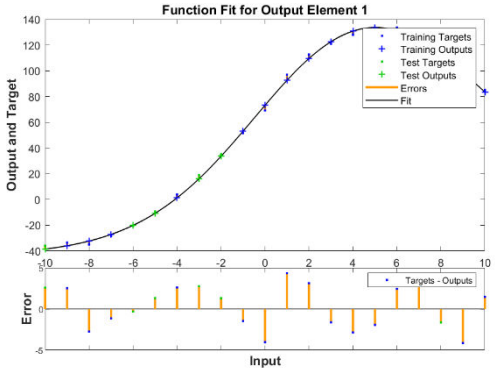

(d) FC

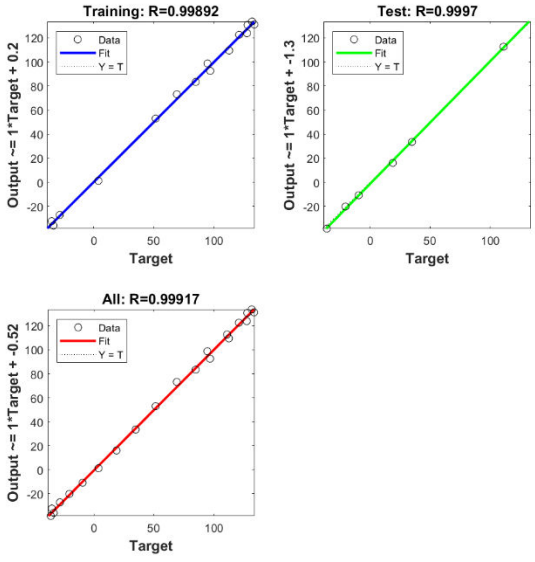

(e) RA

Figure 7. BRNNAI simulations for Airfoil NACA4412 on the basis of C_L/C_D vs Alpha(α)

Figure 8(a) The performance of airfoils, like the NACA 4412, is characterized by important aerodynamic data called the lift coefficient (C_L) and the drag coefficient (C_D). A typical airfoil profile with a cambered shape and specific geometrical characteristics is the NACA 4412. The lift coefficient

(C_L) of the NACA 4412 airfoil is a unit of the quantity of lift that the airfoil can offer whenever there is the supply of an airflow. The NACA 4412 design usually produces a large quantity of C_L and it is applicable in various applications such as in the case of aviation in general. It means that it has the ability to generate enough lift to support an aircraft's weight. On the other hand, the NACA 4412 airfoil's drag coefficient (C_D) measures the quantity of aerodynamic drag it produces when in flight. A lower C_D is preferable as it suggests less airflow resistance, enabling more effective flying. Relatively low C_D of the NACA 4412 is recognized for improving overall performance and fuel economy. In conclusion, the NACA 4412 airfoil is a well-liked option for aircraft design when effective lift generation and drag reduction is essential because it provides an optimal balance of lift (C_L) and drag (C_D) coefficients. α vs C_L illustrates in Figure 8(c). The NACA 4412 airfoil's α vs. C_L graph normally displays a rising C_L with α, peaking at the ideal angle of attack (α_{max}). After this, as the airfoil gets closer and passes through the stall condition, C_L decreases. This graph aids designers and pilots in understanding the aerodynamic' behavior of the airfoil at various α by offering insightful information about the lift characteristics of the airfoil. Figure 8(e) shows the behaviors of α vs C_D. The NACA 4412 airfoil's alpha vs. C_D graph usually shows a region of increasing C_D as the airfoil approaches and passes through the stall, a sharp increase in C_D after the stall, and a generally low and constant C_D at small angles of attack. This graph helps designers and pilots understand the aerodynamic behavior of the airfoil under various conditions by providing important information about the airfoil's performance at different angles of attack. Figure 8(g) shows the behaviors of α vs C_l/C_D. The C_L/C_D ratio normally increases with inclination of α on the C_L/C_D vs α graph for the NACA 4412 airfoil, peaking or plateauing at the α where the maximum L/D ratio is achieved. After this, as the airfoil gets closer to and passes through the stall condition, the C_L/C_D ratio starts to drop. This graph helps designers and pilots optimize the performance of the airfoil for particular applications by showing how effective it is at producing lift in relation to drag at various angles of attack. Figure 8 (b, d, f, h) shows the absolute error plots for C_D vs C_L, α vs C_L, C_D vs α and α vs C_L/C_D, $10^1 \rightarrow 10^{-4}$, $10^{-2} \rightarrow 10^{-5}$, $10^{-3} \rightarrow 10^{-7}$ and $10^1 \rightarrow 10^{-1}$ are noticed respectively.

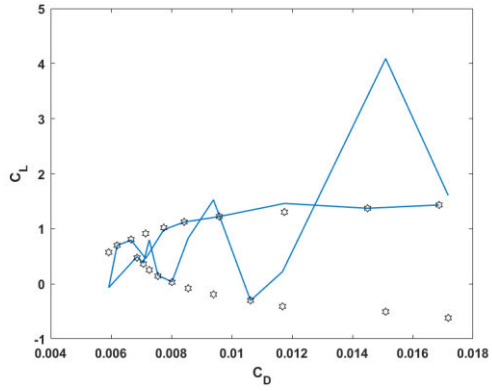

(a) C_D vs C_L

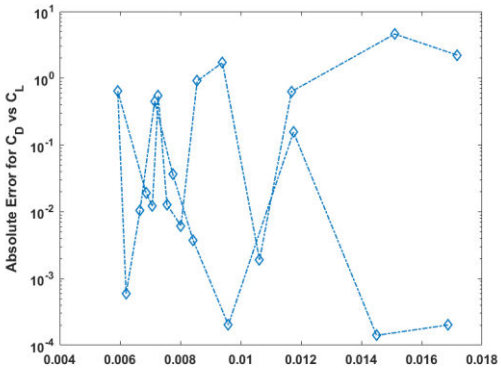

(b) AE for C_D vs C_L

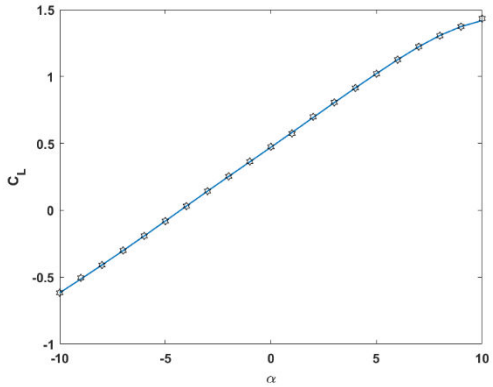

(c) α vs C_L

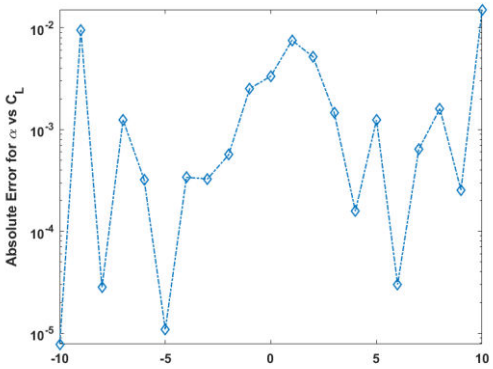

(d) AE for α vs C_L

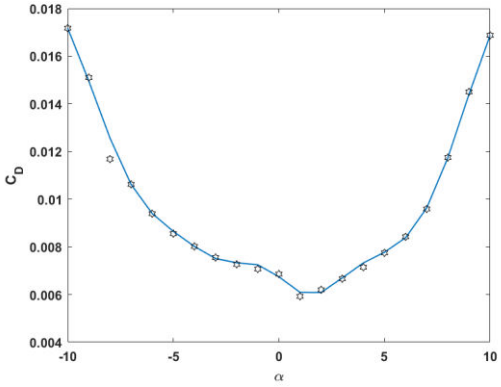

(e) C_D vs α

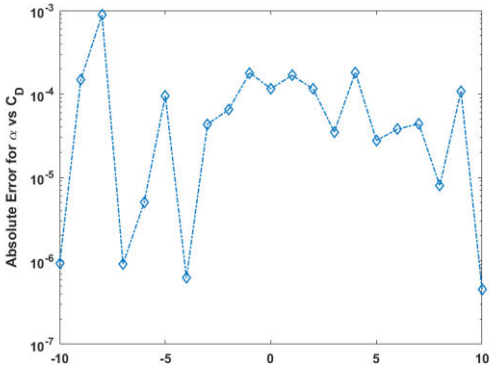

(f) AE for C_D vs α

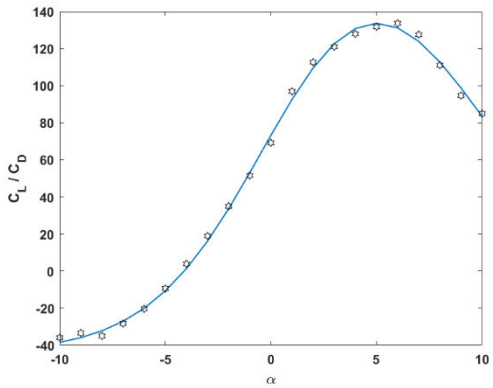

(g) C_L/C_D vs α

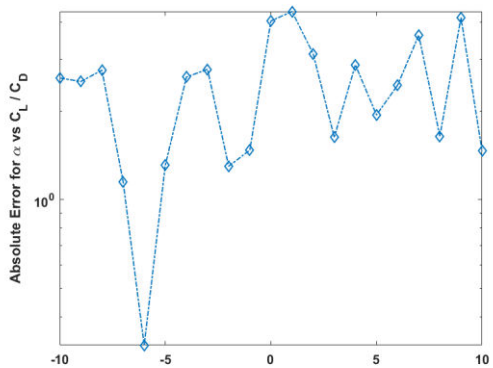

(h) AE for C_L/C_D vs α

Figure 8. Analysis of Airfoil of NACA4412 with their corresponding absolute error plots

3.5. Comparison of NACA 4412 for Subsonic and Transonic Flow

By applying same procedure as mentioned above i.e., firstly we analyze NACA 4412 in XFLR5 for Reynold's number 10^5 with NCrit 9.00 and generated the dataset by the variation of Mach number. As we know that the range of Mach number for subsonic and transonic is < 0.8 and $0.8 - 1.2$ respectively. Then Mach number for subsonic flow is selected 0.0 whereas for transonic flow 0.81 is Mach number. Then by applying neural networks i.e., ANN's Bayesian Regularization technique we got the main plots and absolute error plot which is shown in Figure 9. Figure 9 (a, c) illustrates the analysis of NACA 4412 on the basis of pitch moment coefficient (C_m) and angle of attack (α) which shows that stability of airfoil. Whereas corresponding absolute error for both cases are illustrated in Figure 9 (b, d) respectively. By analyzing both cases we got that NACA 4412 performs better in subsonic flow means on smaller Mach number considered airfoil performs better.

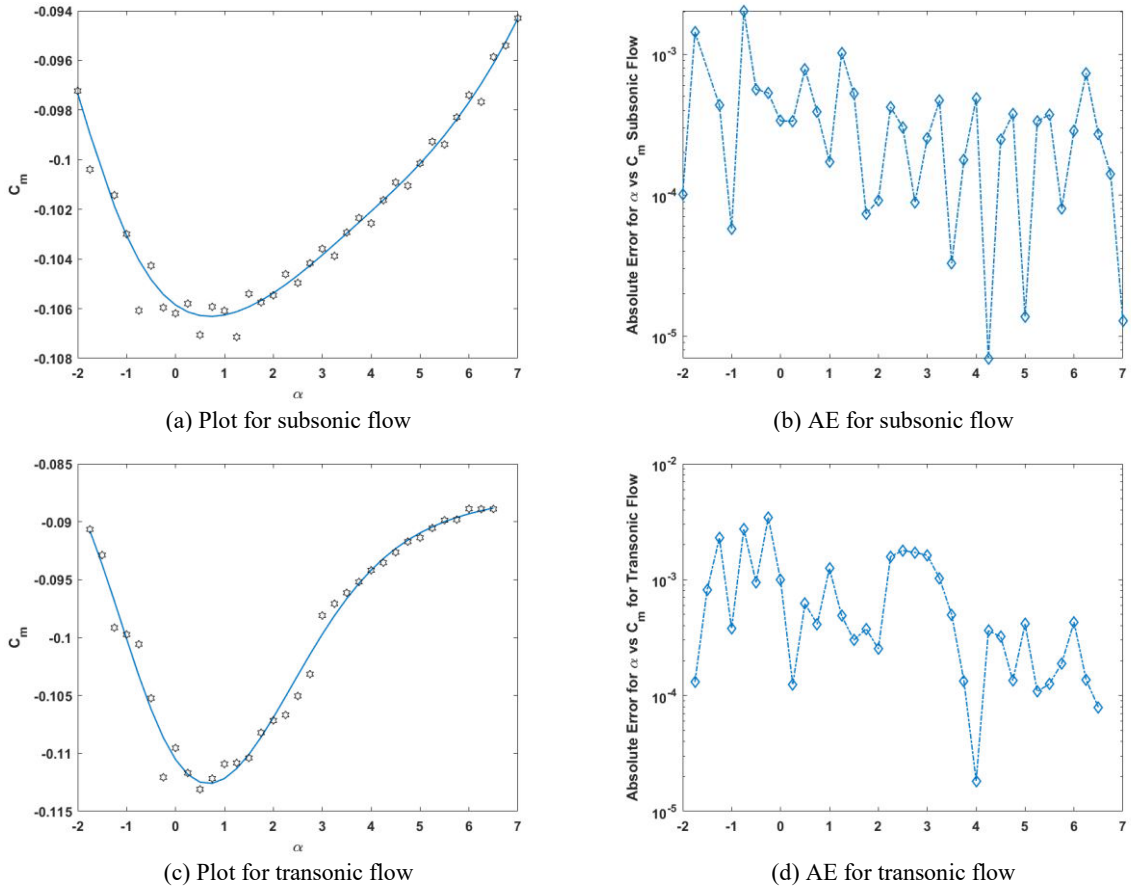

(a) Plot for subsonic flow

(b) AE for subsonic flow

(c) Plot for transonic flow

(d) AE for transonic flow

Figure 9. Analysis of Airfoil of NACA4412 with their corresponding absolute error plots

3.6. Performance Metrics

These are the indices that measure the correspondence between the reference (exact or numerical) XFLR5 data and the BRNNAI predicted solution.

$$MAE = \frac{1}{n}\sum_{i=1}^{n}|y_i - \hat{y}_i| \tag{4}$$

$$RMSE = \sqrt{\frac{1}{n}\sum_{i=1}^{n}(y_i - \hat{y}_i)^2} \tag{5}$$

$$R^2 = \frac{\sum_{i=1}^{n}(y_i-\bar{y})(\hat{y}_i-\bar{\hat{y}})}{\sqrt{\sum_{i=1}^{n}(y_i-\bar{y})^2\sum_{i=1}^{n}(\hat{y}_i-\bar{\hat{y}})^2}} \tag{6}$$

Here, n is the number of the points of the grid, y is original values, $\hat{y}$ is predicted values, $\bar{y} = \frac{1}{n}\sum_{i=1}^{n} y_i$ and $\bar{\hat{y}} = \frac{1}{n}\sum_{i=1}^{n} \hat{y}_i$.

These powerful metrics for performance evaluation are essential to be able to detect the dominant trends and patterns related to the accuracy, robustness, and effectiveness of the model assessments under the best conditions. MSE, RMSE, MAE, MAPE, and R^2 are very good indicators of the level of the difference between real and the measured values. Lower MAE/RMSE and higher R^2 indicate better agreement (see Table 8). Table 8 provide a clear picture of the level of accuracy and the performance of the method proposed.

Table 8. Error Metrics

Parameter	MAE	RMSE	R^2
C_L	0.0021	0.0035	0.998
C_D	0.0008	0.0012	0.996
C_m	0.0015	0.0022	0.995

The performance of the proposed ANN surrogate model was evaluated in terms of prediction accuracy, generalization capability, and consistency with known aerodynamic behavior. The predicted lift coefficient (C_L) exhibits a nearly linear variation with angle of attack in the pre-stall region, followed by a gradual deviation as the stall angle is approached. The measured stall angle of between about $\alpha = 12°$ and 15°, makes sense considering the published aerodynamic experiments concerning NACA 4412 airfoil. Drag coefficient (C_D) is small at low angles of attack and it increases to a large value in and above the stall because of the effects of flow separation. Equally, lift to drag ratio (C_L/C_D) will be highest at moderate angle of attack which implies maximum aerodynamic efficiency. The coefficient of pitching moment (C_m) that has been measured along the quarter-chord in the circular plane has a dominant negative slope with respect to the angle of attack, which indicates that the behavior is statically steady in a flow of incompressible fluid. Statistical anomalies in larger datasets of Mach-number are explained by the inability of the underlying panel analysis to represent the compressibility factors. ANN model has a good predictive performance within all aerodynamic coefficients. A high coefficient of determination (R^2>0.99) and low values of error-denoting variables indicate that the model indeed represents the nonlinear correlation between the input parameters and the aerodynamic outputs. The sensitivity analysis indicates a significant performance of the model as the number of hidden neurons increases in terms of a maximum and optimal number of 20 and above no significant increase is registered. Overall, the results confirm that the ANN model serves as an effective surrogate for approximating aerodynamic datasets, providing rapid predictions with minimal computational cost.

3.7. Limitations

It should be noted that XFLR5 is based on potential flow panel methods with viscous corrections derived from XFOIL. Although it provides reliable predictions for low-Reynolds-number aerodynamic analysis, it does not fully capture compressibility effects or shock wave phenomena associated with true transonic flow. Therefore, the results presented in this study should be interpreted as ANN approximation of aerodynamic datasets generated by XFLR5, rather than high-fidelity compressible flow simulations. Future work will incorporate high-fidelity CFD and experimental datasets to further validate the proposed surrogate modeling framework.

4. Conclusions

In this study, a Bayesian Regularized Artificial Neural Network was developed as a data-driven surrogate model to predict the aerodynamic characteristics of the NACA 4412 airfoil. Aerodynamic data produced with XFLR5 in various flow conditions were used to train the model. The results indicate that the ANN model can be used to approximately estimate the lift, drag, and the pitching-moments coefficient with high levels of correlation and little error in the prediction. The sensitivity test confirmed that the choice of the network architecture and the training parameters is a decisive factor in determining the optimal performance. Aerodynamic trends calculated by the model such as the lift curve behavior, stall behavior, and the change in drag were observed to be in line with known literature, which

demonstrates the effectiveness of the method. It should be noted though that the model is also trained on data that is based in panel-method-based data and fails to take into consideration compressibility effects related to high-speed flows. Thus, the results need to be viewed under the constraints of the data. Further research will be dedicated to the expansion of the suggested framework using high-fidelity CFD simulations and experimental data and the use of the model to solve the aerodynamic optimization problems.

Declarations

Conflict of Interest: None

Funding: None

Data Availability Statement: Data can be made available on reasonable request.

Nomenclature

Latin symbols

Symbol	Definition	Unit
A	Reference area used in the aerodynamic coefficients	[m²]
C_D	Drag coefficient	[–]
C_L	Lift coefficient	[–]
C_L/C_D	Lift-to-drag ratio	[–]
C_m	Pitching moment coefficient	[–]
D	Drag force	[N]
i	Data-point index	[–]
L	Lift force	[N]
n	Number of points used in the performance metrics	[–]
N_{crit}	Critical amplification factor in XFLR5	[–]
Re	Reynolds number	[–]
V	Flow speed	[m s⁻¹]
y_i	Reference value of an aerodynamic coefficient	[–]
$\hat{y}_i$	Predicted value of an aerodynamic coefficient	[–]
$\bar{y}$	Mean reference value	[–]
$\bar{\hat{y}}$	Mean predicted value	[–]

Greek symbols

Symbol	Definition	Unit
α	Angle of attack	[°]
ρ	Fluid density	[kg m⁻³]

Subscripts

Symbol	Definition
crit	Critical amplification factor
D	Drag
i	Data-point index
L	Lift
m	Pitching moment

Abbreviations

Abbreviation	Definition
AE	Absolute error
ANN	Artificial neural network

Abbreviation	Definition
AOA	Angle of attack
BRA	Bayesian regularization approach
BRNNAI	Bayesian regularization based neural-network approach
EH	Error histogram
LSB	Laminar separation bubble
MAE	Mean absolute error
MSE	Mean square error
NACA	National Advisory Committee for Aeronautics
ReLU	Rectified linear unit
RMSE	Root mean square error

References

Aamir, M., Alshehery, S., Abbasi, A. Z., Sohail, M. U., Khan, N., Mesloub, A., Sattar, M., and Kolsi, L. 2025. Analysis for 3D thermal conducting micropolar nanofluid via artificial neural network. *The European Physical Journal Plus*, *140*(2), 100.

Aamir, M., Ghachem, K., Abbasi, A. Z., Eladeb, A., and Kolsi, L. 2026. A quantum neural network approach for high-fidelity simulation of heat and reactive transport of 3D Carreau fluid system. *Multidiscipline Modeling in Materials and Structures*, 1-31.

Abbasi, A. Z., Aamir, M., Sattar, M., Abdullah, N., Abdennaji, T. S., Alshammri, B. M., and Kolsi, L. 2025a. Modeling and prediction of 3D carreau fluid behavior using machine learning for Cattaneo Christov Double diffusion with variable conductivity. *Case Studies in Thermal Engineering*, *72*, 106302.

Abbasi, A. Z., Jaghdam, I. H., Aoudia, M., Maatki, C., Hassen, W., and Kolsi, L. 2025b. Hybrid GA-SQP neural network frame for solving english language learning. *Scientific Reports*, *15*(1), 36450.

Abbasi, A. Z., Aamir, M., Safra, I., Becheikh, N., Kolsi, L., 2026. Quantum-Inspired Intelligent Modeling of Radiative Magneto-Carreau Nanofluid Flow with 3D Unsteady Effects. *International Journal of Modern Physics C*, 2643003. https://doi.org/10.1142/S0129183126430035

Alam, M. and Sandham, N.D., 2000. Direct numerical simulation of 'short'laminar separation bubbles with turbulent reattachment. *Journal of Fluid Mechanics*, *410*, pp.1-28.

Carmichael, B.H., 1981. *Low Reynolds number airfoil survey, volume 1* (No. NASA-CR-165803-VOL-1).

Clausen, P.D. and Wood, D.H., 1999. Research and development issues for small wind turbines. *Renewable energy*, *16*(1-4), pp.922-927.

Genç, M. S. (Ed.), 2012. *Low Reynolds Number: Aerodynamics and Transition*. BoD–Books on Demand.

Genç, M.S., Karasu, İ. and Açıkel, H.H., 2012. An experimental study on aerodynamics of NACA2415 aerofoil at low Re numbers. *Experimental Thermal and Fluid Science*, *39*, pp.252-264.

Hu, H., Yang, Z., 2008. An experimental study of the laminar flow separation on a low-Reynolds-number airfoil. *Journal of Fluids Engineering* 130(5), 051101. https://doi.org/10.1115/1.2907416

Kaldellis, J.K. and Kapsali, M., 2013. Shifting towards offshore wind energy—Recent activity and future development. *Energy policy*, *53*, pp.136-148.

Ledo, L., Kosasih, P.B. and Cooper, P., 2011. Roof mounting site analysis for micro-wind turbines. *Renewable energy*, *36*(5), pp.1379-1391.

Miley, S.J., 1982. *Catalog of low-Reynolds-number airfoil data for wind-turbine applications* (No. RFP-3387). Rockwell International Corp., Golden, CO (USA). Rocky Flats Plant; Texas A and M Univ., College Station (USA). Dept. of Aerospace Engineering.

O'Meara, M.M. and Mueller, T.J., 1987. Laminar separation bubble characteristics on an airfoil at low Reynolds numbers. *AIAA journal*, *25*(8), pp.1033-1041.

Raja, M. A. Z., Abbasi, A. Z., Nisar, K. S., Rafiq, A., Shoaib, M., 2025. A Design of Predictive Intelligent Networks for the Analysis of Fractional Model of TB-Virus. *Computer Modeling in Engineering & Sciences* 143(2), 2133–2153. https://doi.org/10.32604/cmes.2025.058020

Sahin, M., Hall, J., Mohseni, K., Hillewaert, K., 2008, January. Direct numerical simulation of separated low-Reynolds number flows around an Eppler 387 airfoil. In *46th AIAA Aerospace Sciences Meeting and Exhibit* (p. 422).

Shoaib, M., Abbasi, A.Z., Raja, M.A.Z. and Nisar, K.S., 2022. A design of predictive computational network for the analysis of fractional epidemical predictor-prey model. *Chaos, Solitons & Fractals*, *165*, p.112812.

Wahidi, R. and Bridges, D., 2009, June. Experimental investigation of the boundary layer and pressure measurements on airfoils with laminar separation bubbles. In *39th AIAA Fluid Dynamics Conference* (p. 4278).

Wahidi, R., Lai, W., Hubner, J.P. and Lang, A., 2012, July. Volumetric three-component velocimetry and PIV measurements of Laminar Separation Bubbles on a NACA4412 Airfoil. In *16th Int. Symp of applications of laser techniques of fluid mechanics*.

Yarusevych, S., Sullivan, P. and Kawall, J., 2004. Investigation of airfoil boundary layer and wake development at low Reynolds numbers. In *34th AIAA Fluid Dynamics Conference and Exhibit* (p. 2551).